Electron transport properties of calix[4]arene based systems in a metal–molecule–metal junction†

Giuseppe Arena,*[a] Ioannis Deretzis,[b] Giuseppe Forte,[a] Filippo Giannazzo,[b] Antonino La Magna,[b] Giuseppe Lombardo,[a] Vito Raineri,[b] Carmelo Sgarlata[a] and Giuseppe Spoto*[ac]

Received (in Durham, UK) 6th November 2006, Accepted 22nd February 2007
First published as an Advance Article on the web 22nd March 2007
DOI: 10.1039/b616208h

The *I–V* behavior of self-assembled monolayers of a 1,3-alternate bis(dipyridyl)calix[4]arene derivative and its Cu^{2+} complex have been studied by conducting-atomic force microscopy; theoretical calculations have been carried out to simulate *I–V* curves. The experimental data show that the two systems have different conductive properties, the Cu^{2+} complex monolayer having a lower resistance. Theoretical calculations demonstrate that the difference between the two simulated systems results from the different position of their Fermi level. Such a different response to charge transfer may be of interest for the fabrication of molecular electronics devices based on calixarenes.

Introduction

It is commonly believed that the dawn of molecular electronics dates back to the publication of a paper by Aviram and Ratner.[1] This paper described a molecular rectifier based on a molecular tunnelling junction and paved the way to using molecules as electronic components. Over the past couple of decades a sizable body of both experimental and theoretical data has accumulated in the area of molecular electronics[2–6] and the experience thus gained has demonstrated that the ability to switch a molecular property is of paramount relevance for the design and development of new nanodevices.[7] Metal complexes have also been proposed as switches, which can be operated through external inputs (*e.g.* voltage or light).[8]

To the best of our knowledge, very few synthetic systems that change their oxidation state easily have actually been incorporated in metal–molecule–metal types of junctions, in addition to phthalocyanines and porphyrins.[9]

We have studied in detail the Cu^{2+} complexes of 25,27-bis(1-propyloxy)-26,28-bis(2,2′-dipyridyl-6-methoxy)calix[4]-arene in the 1,3-alternate conformation (**CBP**, Scheme 1).[10,11] This system meets the four criteria (*i.e.* size, assembly and recognition, dynamic stereochemistry and synthetic tailorability) that make molecules ideal for electronics applications.[6] ESR and UV-Vis data in the liquid phase clearly indicate that in the $[Cu(\mathbf{CBP})]^{2+}$ species the nitrogen atoms of the dipyridyl substituents are tetrahedrally arranged around the Cu^{2+} ion. This peculiar arrangement accounts for the easy reversible reduction of $[Cu(\mathbf{CBP})]^{2+}$ to $[Cu(\mathbf{CBP})]^{+}$, which makes these systems also good candidates for nanoswitches. Dialkyl sulfide pendants were then introduced into the **CBP** structure; the resulting ligand (25,27-bis[12-(thiododecyl)undecyloxy]-26,28-bis(2,2′-dipyridyl-6-methoxy)calix[4]arene 1,3-alternate, **CBPS**, Scheme 1) easily self-assembled onto Au(111) surfaces. A coupled PM-IRRAS and FT-SPR study showed that **CBPS** forms well ordered SAMs and is able to complex Cu^{2+}, when exposed to Cu^{2+} solutions.[12]

However, it is widely recognized that a key challenge in molecular electronics is to translate the solution-phase properties into solid-state device settings.[6] In addition, until a common analytical tool that can be used to correlate the structure and dynamics of molecules in the solution-phase with the characteristics of solid-state molecular electronic devices is developed, investigating how the performance of a device may be modified through molecular structure variations seems to be the only way to contribute to the understanding of the way junctions work.[7,13]

We have now sandwiched both the bare ligand (**CBPS**) and its Cu^{2+} complex ($[Cu(\mathbf{CBPS})]^{2+}$) in a metal–molecule–metal junction made by contacting Au-supported self assembled monolayers of either **CBPS** or $[Cu(\mathbf{CBPS})]^{2+}$ with a conducting AFM tip. AFM-based measurements have the advantage of being relatively simple; they also are a good way to overcome the synthetic steps that can damage or unpredictably modify the molecular system.[14,15] The characterization and properties of these two junctions are described here. The widely recognized need[7,16,17] to interpret the experimentally determined properties of the junction has prompted us to model the *I–V* curve of the two junctions through theoretical semi-empirical methods. These methods have the advantage of being fairly flexible, simple and computationally inexpensive, while at the same time quantitatively accurate, especially for

[a] *Dipartimento di Scienze Chimiche, Università di Catania, Viale A. Doria 6, 95125 Catania, Italy*
[b] *Istituto per la Microelettronica e Microsistemi, CNR, Sezione di Catania, Stradale Primosole 50, 95121 Catania, Italy*
[c] *Istituto Biostrutture e Bioimmagini, CNR, Viale A. Doria 6, 95125 Catania, Italy*

† Dedicated to Professor George Gokel on the occasion of his 60th birthday.

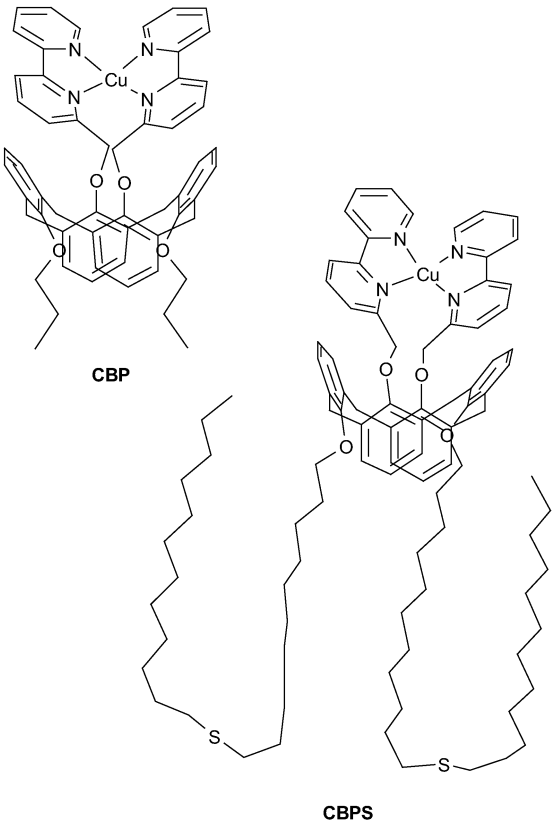

Scheme 1

cases in which a proper parameterization of independent variables cannot be solely attained *via* the theoretical approach (*e.g.* applying *ab initio* methods).

Results and discussion

Monolayer properties and current–voltage behaviour

Some of the properties of **CBPS** and $[Cu(\mathbf{CBPS})]^{2+}$ monolayers have been presented elsewhere.[12] In particular, it was demonstrated that **CBPS** forms well-ordered monolayers on Au(111) surfaces and that Cu^{2+} can be complexed by the anchored receptor. Moreover, it was shown that an appropriate Cu^{2+} analytical concentration is needed to guarantee the formation of a 1 : 1 metal–receptor complex.[11]

Fig. 1 shows a set of 16 different curves representing the typical forward and reverse current–voltage (*I–V*) curve obtained when an Au coated Si_3N_4 tip was brought in contact with the **CBPS** monolayer. The curves shown in Fig. 1 refer to the *I–V* curves obtained by probing 16 different positions within a 4 × 4 matrix with 200 nm steps. The applied load was 20 nN. Fig. 1 shows that *I–V* dependence is sigmoidal over the ±3 V range while it is linear over the ±0.3 V interval (inset A). The forward and reverse curves resulting from the average of the 16 experimental curves are shown in inset B. An average junction resistance of about 1.7×10^{11} Ω was calculated by considering the inverse of the slope of the linear region of the *I–V* plot.[14b] Replicates and independent experiments showed

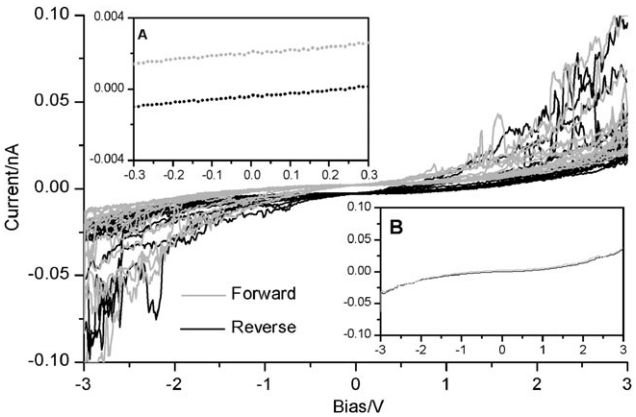

Fig. 1 *I–V* curves for **CBPS** monolayers; 16 different positions of a 4 × 4 matrix with 200 nm steps were probed. The forward and reverse curves resulting from the average of the 16 experimental curves are shown in inset **B**. The ±0.3 V interval where the *I–V* relation is linear is shown in inset **A**.

the fundamental role played by Au(111) surface reconstruction. *I–V* curves were hardly reproducible when **CBPS** monolayers anchored onto unreconstructed Au(111) surfaces were used. Moreover, correct settings for both voltage sweep ranges and tip loads were required to ensure the monolayer conducting properties. Typically, voltage excursions beyond 3 V together with tip loads over 20 nN caused an irreversible junction breakdown, which produced a dramatic increase in the measured current.

It is noteworthy that the monolayer surface coverage (0.55 molecules nm^{-2}), estimated by FT-SPR experiments, rules out a contact between the tip probe and the metallic layer of the Au(111) substrate. Such a coverage value, together with an estimated tip contact area,[18] of about 6 nm^2 indicates that the junction involves approximately 3 molecules.

Fig. 2 shows a set of 16 different curves representing the typical forward and reverse *I–V* curves obtained when the Au coated tip was brought in contact with 16 different positions of the $[Cu(\mathbf{CBPS})]^{2+}$ monolayer. Similarly to **CBPS,** 16 different positions were explored (a 4 × 4 matrix with 200 nm steps).

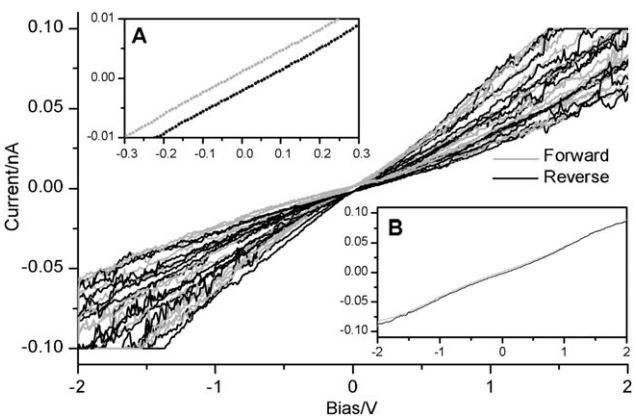

Fig. 2 *I–V* curves for $[Cu(\mathbf{CBPS})]^{2+}$ monolayers; 16 different positions of a 4 × 4 matrix with 200 nm steps were probed. The ±0.3 V interval where the *I–V* relation is linear and the average *I–V* curves are shown in insets **A** and **B**, respectively.

Also in this case a tip load of 20 nN was applied as it was experimentally verified that junction breakdown occurred with higher tip loadings. The curves obtained for the $[Cu(\mathbf{CBPS})]^{2+}$ differ markedly from those obtained for **CBPS** and indicate a more resistive behaviour in the latter case. The ± 0.3 V region, where the *I–V* curve is linear (inset A), was used to estimate the junction resistance for the $[Cu(\mathbf{CBPS})]^{2+}$ monolayer which turned out to be approximately 2.9×10^{10} Ω.

Theoretical calculations

Molecular modeling optimized structures of both **CBPS** and $[Cu(\mathbf{CBPS})]^{2+}$ were used to set up the 'two-terminal' system used for the theoretical electronic transport calculations.[19] A non-equilibrium Green's functional formalism with an extended Hückel Hamiltonian was used to model the metal–molecule–metal experimental system (see Experimental section). In particular, the two molecular structures were 'sandwiched' between two semi-infinite Au(111) contacts, one of which represents the Au(111) substrate onto which the molecular system was immobilized through its dialkyl sulfide moieties, while the other one represents the gold coated AFM tip. The distance between the molecular system and the metallic pads was set at 0.2 nm. Having fixed the contact–molecule distance, a further investigation of the relative positioning between interface molecular and metallic atoms was not carried out, since a variation of the latter could only marginally affect the transport characteristics of the studied system.[20]

The theoretical simulation was focused on the system transmission functions as well as on the calculated *I–V* trend. Fig. 3 shows the transmission functions calculated for both the **CBPS** and $[Cu(\mathbf{CBPS})]^{2+}$. The results reveal a low transmission probability in the Fermi energy region (E_F(Au) = −9.5 eV) of the gold contacts. The transmission properties of the studied systems are strongly influenced by the transport properties of the two dialkyl sulfide moieties present in the structure (Fig. 3). Indeed, the two sides of the wide transmission gap correspond to the two energy regions near the HOMO and LUMO levels of the dialkyl sulfide chains. The set of localized states due to the **CBPS** structure that fall in this energy range do not contribute significantly to the transmission of the systems. However, the overall trend of the transmission spectrum does not change substantially following Cu^{2+} complexation as indicated by both the overall trend of the two spectra and the similarity of both the gaps between two spectral regions with high transmission (~14 eV). Thus, a more detailed analysis was therefore needed to theoretically interpret the difference between the *I–V* curves experimentally obtained for **CBPS** and $[Cu(\mathbf{CBPS})]^{2+}$ monolayers.

Indeed, the inclusion of an impurity may modify the transport features of a molecular system due to two possible (and sometimes concurrent) effects: (a) a change in the transmission spectrum related to a different distribution of the eigenvalues of the system (this effect is weak in our case), (b) a change in the Fermi energy level E_F of the composite system (pads + device) due to ion-induced charging. Varying E_F results in a change of the system resistance since it moves the effective integration interval (*namely*, where $f(E,\mu_L) - f(E,\mu_R) \neq 0$) from the low to the high transmission region of the spectrum

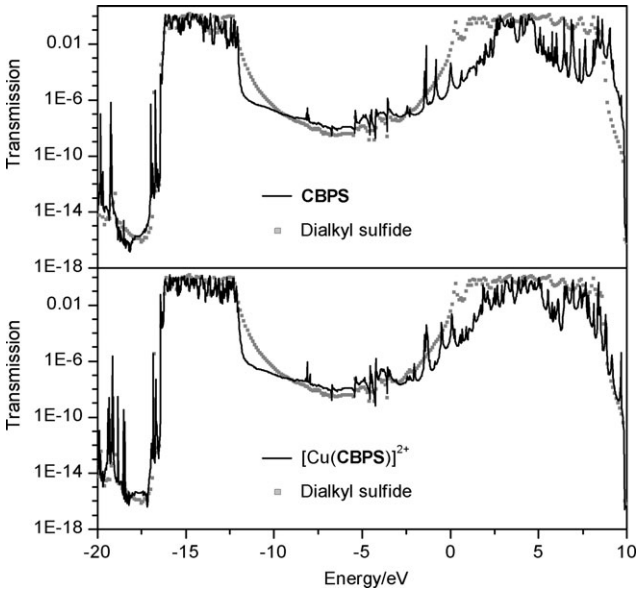

Fig. 3 Transmission as a function of the energy for **CBPS**, $[Cu(\mathbf{CBPS})]^{2+}$ and dialkyl sulfide.

or *vice versa*, as easily shown by Landauer's equation (eqn (2), see later). Since the transmission spectra for **CBPS** and $[Cu(\mathbf{CBPS})]^{2+}$ are similar, the effect of the E_F change has to be significant in our case and this likely accounts for the modification of the *I–V* characteristics observed in the presence of copper, as discussed below.

As we stated above, the conducting behavior of a system (pads + device) is highly dependent on the value of its equilibrium electrochemical potential (*i.e.* the Fermi energy level), which is situated within the HOMO–LUMO levels.[21] The extended Hückel model used in this study does not calculate self-consistently the Fermi energy level of the system investigated, in agreement with other semi empirical approaches. Errors for systems with large conduction gaps may show up even if more sophisticated *ab initio* approaches are used. In this context, the Fermi level energy is set as an adjustable parameter in the extended Hückel model and it is allowed to vary in order to obtain the best overlap with the experimental curves.[17] Such a procedure is commonly adopted for Si-based transistors; adjusting the Fermi level in the transport simulations makes it possible to take into account uncertainties arising from unexpected interface reconstruction, presence of surface impurities, *etc*. Fig. 4 and 5 show both the experimental (gray lines) as well as the theoretical (black and dotted lines) *I–V* curves for the **CBPS** and $[Cu(\mathbf{CBPS})]^{2+}$ system, respectively. The different theoretical curves were obtained by setting the Fermi level position as the only variable parameter. The theoretical *I–V* curves, obtained by setting the Fermi level energy at the known value for gold (E_F(Au) = −9.5 eV), are also shown in Fig. 4 and 5. Interestingly, a better agreement between the theoretical and experimental curves is obtained by fixing the Fermi level energy at values which are different not only from the E_F = −9.5 eV value expected for pure gold contacts but also from one another. In fact E_F values of −8.5 eV and −10.85 eV are required for an optimal overlap of the *I–V* curves obtained for

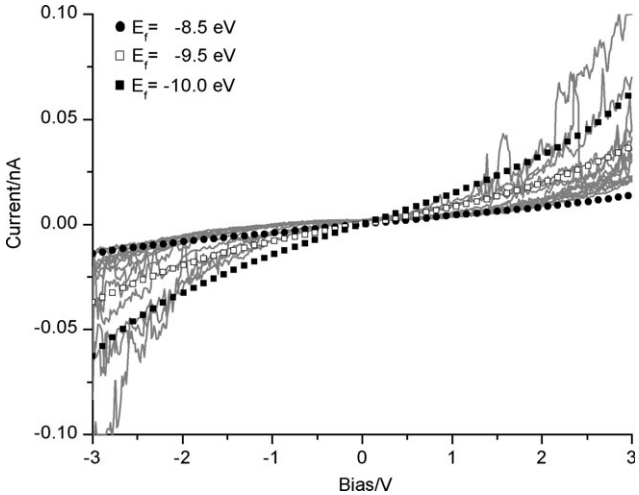

Fig. 4 Theoretical *I–V* curves obtained for **CBPS** with three different values of the Fermi level energy. Theoretical *I–V* curves overlap with experimental *I–V* curves optimally when the Fermi level is set at $E_F = -8.5$ eV. A theoretical *I–V* curve, obtained by setting the Fermi level at the well known value for gold ($E_F = -9.5$ eV), is also shown for comparison.

the **CBPS** and $[Cu(\mathbf{CBPS})]^{2+}$ monolayers, respectively. The significant difference in the theoretical Fermi level position ($E_F = -8.50$ eV for the **CBPS** and $E_F = -10.85$ eV $[Cu(\mathbf{CBPS})]^{2+}$) results from the actual change of the local electrochemical potential of the two molecules which causes a different charge transfer from and to the gold contacts.

Conclusions

The practical use of molecular systems for the fabrication of solid-state devices requires a deep knowledge of the fundamental properties of the molecular system in the same conditions where it is planned to be used. **CBPS** and its Cu^{2+} complex immobilized onto Au(111) surfaces form monolayers, the conducting behaviour of which has been studied by conducting-AFM. The monolayer conductivity is strongly influenced by the properties of the dialkyl sulfide moieties present in the structures of the molecular receptors. At a first glance both systems show capacitive properties and might be classified as insulators. However, significant differences between **CBPS** and $[Cu(\mathbf{CBPS})]^{2+}$ monolayers are detected which result from the lower resistance of the latter. Theoretical calculations have shown that the different conductive behaviour of the two monolayers results from the presence of the Cu^{2+} that causes a different response of the molecular system to the charge transfer from and to the gold contacts. In conclusion, **CBPS** forms monolayers which can hold the electric charge and the presence of its Cu^{2+} complex yields a molecular device with different electrical properties. Thus, in principle, the metal ion complexation can be considered a way to address different information to the monolayer surface.

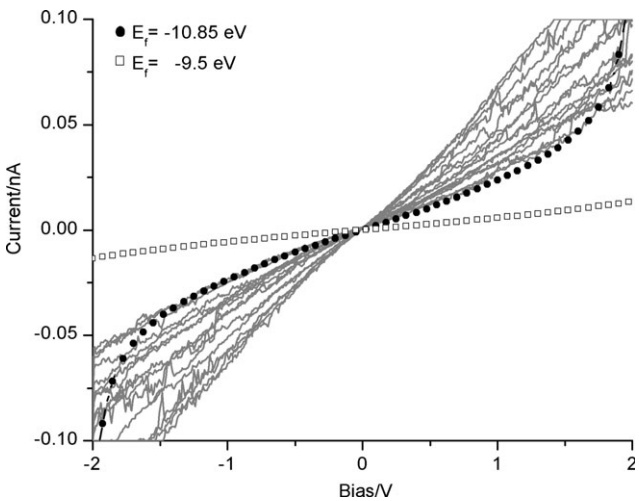

Fig. 5 Theoretical *I–V* curves obtained for $[Cu(\mathbf{CBPS})]^{2+}$ with two different values of the Fermi level energy were considered. Theoretical *I–V* curves overlap with experimental *I–V* curves optimally when the Fermi level is set at $E_F = -10.85$ eV.

Experimental

Monolayer preparation

CBPS was synthesized by following procedures described elsewhere.[12] **CBPS** monolayers were prepared by immersing flame annealed Au(111) substrates (Arrandee, Germany) in a 3×10^{-3} mol dm^{-3} ethanol–chloroform (1 : 1, v/v) solution of the receptor for 24 hours at room temperature under an inert atmosphere. The samples were then removed from the solution and rinsed with large amounts of ethanol and chloroform. $[Cu(\mathbf{CBPS})]^{2+}$ monolayers were obtained by following a similar procedure except that a $[Cu(\mathbf{CBPS})]^{2+}$ solution was used; this was obtained by mixing $Cu(ClO_4)_2$ with the above mentioned **CBPS** solution. The analytical concentration of Cu^{2+} in the final solution (10^{-2} mol dm^{-3}) was chosen as to allow the 1 : 1 complex formation.[11] All glassware used in monolayer preparation was cleaned in piranha solutions (concentrated H_2SO_4 and 33% H_2O_2 in a 3 : 1 v/v ratio) and rinsed with copious amounts of high-purity water (Milli-Q Element Ultrapure Water) before use. *Warning*: piranha solutions should be handled with caution as they can detonate unexpectedly.

Conducting AFM (C-AFM) measurements

All measurements were carried out using a Digital Instruments Dimension 3100 system (Santa Barbara, CA, USA) equipped with a Tunneling AFM (TUNA) module. Commercially available V-shaped Si_3N_4 cantilevers (nominal force constant 0.12 N m^{-1}) were used for the conductive measurements. Tips were coated by sputter deposition of gold until a 10 nm thick layer was obtained and were immediately used for the C-AFM measurements. Tips were never used for more than one day. Junctions were formed by placing the conducting tips in stationary point contact, under controlled load, with the SAM surface. The mechanical load was held constant using standard AFM feedback. Voltages were applied to the Au/SAM substrate; the metallic coated tip was grounded. The tips were not scanned over the surface to avoid damaging the gold coating. Typically, 16 *I–V* curves (scan rate 0.1933 Hz) were obtained from separate areas defined by a 4×4 matrix of points with 200 nm steps.

Fourier transform-surface plasmon resonance (FT-SPR) and surface coverage calculation

FT-SPR experiments were carried out by using an FT-SPR 100 (GWC Instruments, WI, USA) apparatus. The light beam from an external port of a Nexus 870 FT-IR spectrometer (Nicolet, WI, USA), equipped with a quartz–halogen source and a XT-KBr beam splitter, was used as the near-IR source for the FT-SPR. Gold substrates (GWC Instruments, WI, USA) were obtained by thermally evaporating a gold layer (45 nm) on to SF-10 glass slides. Chromium (5 nm) was used as the adhesion layer. Gold substrates were brought into optical contact with the SF-10 equilateral prism present in the FT-SPR by using a refractive index matching fluid (Cargille Laboratories, USA). FT-SPR experiments were carried out by using a 60 μl flow cell (GWC Technologies, MD, USA) and an IPC-N (Ismatec, Switzerland) peristaltic pump.

The FT-SPR sensor signal was converted into refractive index changes by using independent sucrose aqueous calibrating solutions ($r^2 = 0.999$). The refractive indexes of the sucrose solutions were obtained from the literature.[22]

FT-SPR was used to estimate the monolayer surface coverage by following a method described in the literature.[23] According to this method, the adlayer thickness (d) is obtained from the measured FT-SPR signal, that is, the shift in wavenumber of the FT-SPR minimum in reflected light intensity associated with changes in the index of refraction of the medium in contact with the metal surface of the FT-SPR device. To have more reliable FT-SPR experiments the use of volatile solvents such as chloroform was avoided. For this reason monolayer surface coverage calculations were based on FT-SPR signals obtained by using an ethanol soluble calix[4]-arene-based adsorbate[24] closely resembling **CBPS**. Conclusions drawn from such experiments were considered a reasonable estimate of the **CBPS** monolayer surface coverage. The value of the refractive index of the adsorbate was 1.45,[25] while the value of 1.359 was considered for the refractive index of the pure ethanol.[22]

A 1×10^{-3} M ethanol solution of the adsorbate was eluted in the FT-SPR flow cell at a flow-rate of 10 μl min^{-1} in order to allow its anchoring on the sensor chip surface. Pure ethanol was then introduced into the flow cell after about 16 hours. The FT-SPR shift due to the adsorbate anchoring was determined (Fig. 6) and this led to an adlayer thickness value of $d =$ 1.04. The adlayer thickness may be then easily converted into the surface concentration, θ, (molecules cm^{-2}) using eqn (1):

$$\theta \text{ (molecules cm}^{-2}) = d \text{ (cm)} \times N \text{ (molecules cm}^{-3}) \quad (1)$$

where N is the bulk number density of the adsorbate. N can be calculated by dividing the bulk density of the adsorbate (ρ/g cm^{-3}) by the molecular weight and multiplying the result by Avogadro's number. Introducing in eqn (1) the value for ρ (1.30 g cm^{-3}) reported in the literature[26] leads to a θ value of 5.5×10^{13} molecules cm^{-2} (*i.e.* 0.55 molecules nm^{-2}).

Computational details

Molecular Mechanics (MM) calculations were performed with the Forcite program of the Materials Studio package (Accelrys Inc., San Diego, CA, USA). Molecular structures of both

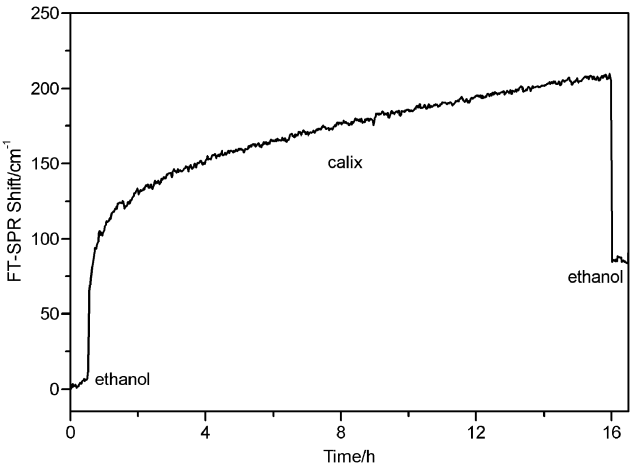

Fig. 6 Change of the FT-SPR minimum with time obtained when the dialkyl sulfide bearing calix[4]arene-based system flows in contact with the Au(111) surface. The change of the FT-SPR signal position before and after flowing the molecular receptor containing solution is used to determine the surface coverage. In the present case a surface coverage of 0.55 molecules nm^{-2} was obtained.

CBPS and its Cu^{2+} complex were optimized with the Universal force field by using the default settings of the program "Smart optimization algorithm" (a cascade of steepest descent, ABNR and quasi-Newton methods) with a convergence threshold set at 0.001 kcal mol^{-1} for the energy and 0.5 kcal mol^{-1} $Å^{-1}$ for the force, respectively; an atom based summation method for the non-bond interactions with cut-off distance of 5 nm and cubic spline truncation was used. Atomic charges were obtained *via* the charge equilibration method.

Theoretical determination of the molecular conductance

The transport properties of both **CBPS** and [Cu(**CBPS**)]$^{2+}$ monolayers were theoretically studied in a 'two-terminal' regime, by means of the non-equilibrium Green's functional formalism with an extended Hückel Hamiltonian.[21] The approach was based on the single particle retarded Green's function matrix $G = [ES - H - \Sigma_L - \Sigma_R]^{-1}$, where H is the 'device' Hamiltonian in an appropriate basis set, S is the overlap matrix in that basis set and $\Sigma_{L,R}$ is the self energy which includes the effect of scattering due to the left (L) and right (R) metallic electrodes. The contact self-energy can be expressed as $\Sigma = \tau g_s \tau^{\dagger}$ where g_s is the Green's function of the contact restricted to the surface zone and τ is the Hamiltonian relative to the mutual interaction between the molecule and the contact. In the case of coherent transport, the current can be calculated directly using a Landauer-type expression (eqn (2)):

$$I = \frac{2e}{h} \int_{-\infty}^{+\infty} dE\, T(E)[f(E,\mu_L) - f(E,\mu_R)] \quad (2)$$

where the transmission is $T(E) = Tr[\Gamma_L G \Gamma_R G^{\dagger}]$ with $\Gamma_{L,R} = i[\Sigma_{L,R} - \Sigma_{L,R}^{\dagger}]$. In eqn (2) $f(E,\mu_{L,R})$ is the Fermi–Dirac distribution of electrons in the contact at chemical potential $\mu_{L,R} = E_F \pm 0.5$ V[17,21] where E_F is the Fermi energy of the system and V the applied potential.

The device and contact electronic behavior is described by the extended Hückel Hamiltonian, which uses all valence electrons as the basis set functions (approximated by Slater-type non-orthogonal orbital functions). The single particle Hamiltonian matrix elements are

$$H_{i,j} = \begin{cases} -V_i & \text{if } i = j \\ \frac{S_{ij}}{2}(V_i + V_j) & \text{if } i \neq j \end{cases}$$

where i and j run over all valence orbitals. The overlap matrix S_{ij} and the diagonal elements V_i can be calculated, given the system's geometry, using the appropriate parameterization.[27] The choice of the Hamiltonian matrix was made by considering the good descriptive capability of the extended Hückel method compared to other semi empirical approaches (*e.g.* single-electron Tight Binding Hamiltonians) in terms of topological and bond strength characteristics of the chemical interactions between intra-molecular as well as interface atoms on the contact region.[20]

Acknowledgements

The authors gratefully acknowledge Mrs Valeria Zito (IBB, CNR) for technical assistance. I.D. and A.L. are grateful to Regione Sicilia (POR-Regione Sicilia—Misura 3.15) for partial financial support. G.A. gratefully acknowledges the University of Catania (Progetto Ateneo 2006) for partial support.

References

1 A. Aviram and M. A. Ratner, *Chem. Phys. Lett.*, 1974, **29**, 277.
2 (*a*) M. A. Reed, C. Zhou, C. J. Muller, T. P. Burgin and J. M. Tour, *Science*, 1997, **278**, 252; (*b*) J. Chen, M. A. Reed, M. A. Rawlett and J. M. Tour, *Science*, 1999, **286**, 1550; (*c*) C. J. Collier, E. W. Wong, M. Belohradsky, F. M. Raymo, J. F. Stoddart, P. J. Kuekes, R. S. Williams and J. R. Heath, *Science*, 1999, **285**, 391.
3 J. H. Schon, H. Meng and Z. Bao, *Nature*, 2001, **413**, 713.
4 (*a*) R. L. Carroll and C. B. Gorman, *Angew. Chem., Int. Ed.*, 2002, **41**, 4378; (*b*) R. A. Wassel and C. B. Gorman, *Angew. Chem., Int. Ed.*, 2004, **43**, 5120.
5 A. Salomon, D. Cahen, S. Lindsay, J. Tomfohr, V. B. Engelkes and C. D. Frisbie, *Adv. Mater.*, 2003, **15**, 1.
6 J. R. Heath and M. A. Ratner, *Phys. Today*, 2003, **56**, 43.
7 (*a*) C. P. Collier, G. Mattersteig, E. W. Wong, Y. Luo, K. Beverly, J. Sampaio, F. M. Raymo, J. F. Stoddart and J. R. Heat, *Science*, 2000, **289**, 1172; (*b*) A. R. Pease, J. O. Jeppesen, J. F. Stoddart, Y. Luo, C. P. Collier and J. R. Heath, *Acc. Chem. Res.*, 2001, **36**, 433.
8 (*a*) P. J. Low, *Dalton Trans.*, 2005, 2821; (*b*) A. C. Benniston, *Chem. Soc. Rev.*, 2004, **33**, 573; (*c*) N. Robertson and C. A. McGowan, *Chem. Soc. Rev.*, 2003, **32**, 96.
9 (*a*) W. Deng and K. W. Hipps, *J. Phys. Chem. B*, 2003, **107**, 10736; (*b*) K. W. Hipps, D. E. Barlow and U. Mazur, *J. Phys. Chem. B*, 2000, **104**, 2444; (*c*) J. Park, A. N. Pasupathy, J. I. Goldsmith, C. Chang, Y. Yaish, J. R. Petta, M. Rinkoski, J. P. Sethna, H. D. Abruna, P. L. McEuen and D. C. Ralph, *Nature*, 2002, **417**, 722; (*d*) G. Maruccio, A. Biasco, P. Visconti, A. Bramanti, P. P. Pompa, F. Calabi, R. Cingolani, R. Rinaldi, S. Corni, R. Di Felice, E. Molinari, M. P. Verbeet and G. W. Canters, *Adv. Mater.*, 2005, **17**, 816; (*e*) N. J. Tao, *Phys. Rev. Lett.*, 1996, **76**, 4066.
10 G. Arena, A. Contino, E. Longo, D. Sciotto, C. Sgarlata and G. Spoto, *Tetrahedron Lett.*, 2003, **44**, 5415.
11 G. Arena, R. P. Bonomo, A. Contino, C. Sgarlata, G. Spoto and G. Tabbí, *Dalton Trans.*, 2004, 3205.
12 G. Arena, A. Contino, E. Longo, C. Sgarlata, G. Spoto and V. Zito, *Chem. Commun.*, 2004, 1812.
13 C. P. Collier, J. O. Jeppesen, Y. Luo, J. Perkins, E. W. Wong, J. R. Heath and J. F. Stoddart, *J. Am. Chem. Soc.*, 2001, **123**, 12632.
14 (*a*) D. J. Wold and C. D. Frisbie, *J. Am. Chem. Soc.*, 2000, **122**, 2970; (*b*) D. J. Wold and C. D. Frisbie, *J. Am. Chem. Soc.*, 2001, **123**, 5549; (*c*) D. J. Wold, R. Haag, M. A. Rampi and C. D. Frisbie, *J. Phys. Chem. B*, 2002, **106**, 2813; (*d*) V. B. Engelkes, J. M. Beebe and C. D. Frisbie, *J. Am. Chem. Soc.*, 2004, **126**, 14287.
15 (*a*) X. D. Cui, A. Primak, X. Zarate, J. Tomfohr, O. F. Sankey, A. L. Moore, T. A. Moore, D. Gust, G. Harris and S. M. Lindsay, *Science*, 2001, **294**, 571; (*b*) X. D. Cui, A. Primak, X. Zarate, J. Tomfohr, O. F. Sankey, A. L. Moore, T. A. Moore, D. Gust, L. A. Nagahara and S. M. Lindsay, *J. Phys. Chem. B*, 2002, **106**, 8609; (*c*) X. D. Cui, X. Zarate, J. Tomfohr, O. F. Sankey, A. Primak, A. L. Moore, T. A. Moore, D. Gust, G. Harris and S. M. Lindsay, *Nanotechnology*, 2002, **13**, 5.
16 S. L. Lindsay, *J. Chem. Educ.*, 2005, **82**, 727.
17 F. Zahid, M. Paulsson, E. Polizzi, A. W. Ghosh, L. Siddiqui and S. Datta, *J. Chem. Phys.*, 2005, **123**, 64707.
18 The radius of the tip contact area can be estimated according to procedures described in ref. 14*b* by considering a tip radius of 10 nm, an applied load of 20 nN and an elastic modulus of the surface of 77 GPa.
19 (*a*) A. K. Rappé, C. J. Casewit, K. S. Colwell, W. A. Goddard and W. M. Skiff, *J. Am. Chem. Soc.*, 1992, **114**, 10024; (*b*) A. K. Rappé, K. S. Colwell and C. J. Casewit, *Inorg. Chem.*, 1993, **32**, 16; (*c*) U. Burkert and N. L. Allinger, *Molecular Mechanics*, American Chemical Society, Washington, 1982.
20 I. Deretzis and A. La Magna, *Nanotechnology*, 2006, **17**, 5063.
21 F. Zahid, M. Paulsson and S. Datta, *Electrical Conduction through Molecules*, in *Advanced Semiconductors and Organic Nano-Techniques*, ed. H. Morkoc, Academic Press, New York, 2003.
22 *Handbook of Chemistry and Physics*, ed. D. R. Lide, 71st edn, CRC Press, Boston, 1990.
23 (*a*) G. Grasso, R. D'Agata, E. Rizzarelli, G. Spoto, L. D'Andrea, C. Pedone, A. Picardi, A. Romanelli, M. Fragai and K. J. Yeo, *J. Mass Spectrom.*, 2005, **40**, 1565; (*b*) L. S. Jung, C. T. Campbell, T. M. Chinowsky, M. N. Mar and S. S. Yee, *Langmuir*, 1998, **14**, 5636.
24 G. Arena, A. Contino, R. D'Agata, C. Sgarlata and G. Spoto, *New J. Chem.*, 2005, **29**, 1393.
25 E. U. Thoden van Velzen, J. F. J. Engbersen, P. J. de Lange, J. W. G. Mahy and D. N. Reinhoudt, *J. Am. Chem. Soc.*, 1995, **117**, 6853.
26 P. A. Anquetil, H. H. Yu, J. D. Madden, P. G. Madden, T. M. Swager and I. W. Hunter, *Proc. SPIE–Int. Soc. Opt. Eng.*, 2002, **4695**, 424.
27 (*a*) R. S. Mulliken, C. A. Rieke, D. Orloff and H. Orloff, *J. Chem. Phys.*, 1949, **17**, 1248; (*b*) R. Hoffmann, *J. Chem. Phys.*, 1963, **39**, 1397.